Thermochimica Acta, 202 (1992) 151–171
Elsevier Science Publishers B.V., Amsterdam

Diffusional limitations on the kinetics of dehydration reactions of hydrated barium chloride

Janice Antoine Lumpkin and Daniel D. Perlmutter

Department of Chemical Engineering, University of Pennsylvania, Philadelphia, PA 19104-6393 (USA)

(Received 10 September 1991)

Abstract

The dehydration kinetics of $BaCl_2 \cdot 2H_2O$ powders were examined as a function of water vapor pressure, sample bed depth, particle diameter and temperature. The conversion behavior was modeled in both the kinetic and the combined diffusion and kinetic limited regimes with modified forms of the Avrami–Erofe'ev equation. Kinetic data were obtained by thermogravimetric techniques and by calorimetry. Structural data for intermediates and products were obtained by X-ray diffraction and optical microscopy. Dehydrations were conducted isothermally between 317 and 335 K either under vacuum or in controlled pure water vapor atmospheres ranging from 40 to 6.67×10^2 Pa.

The dehydration rate decreased as the water vapor pressure, sample bed depth and particle diameter increased. The estimated effective bed diffusivity is 1.0×10^{-6} cm^2 s^{-1}. After a critical pressure was exceeded, severe reductions in rate were observed. The dehydration of $BaCl_2 \cdot 2H_2O$ proceeded stepwise via the crystalline monohydrate above about 80 Pa at 317 K; below this pressure the crystalline monohydrate was not observed. Transient increases in water vapor pressure in the sample bed caused crystallization of the monohydrate under conditions where it did not otherwise form.

INTRODUCTION

Thermal dehydration of a crystalline hydrate is one of the simplest reactions of the class of decompositions

$$A(s) \rightarrow B(s) + C(g)$$

Although this relative simplicity has been exploited to provide valuable information concerning the nature of non-catalytic solid state reactions [1], complex parametric sensitivities exist which are still not fully understood. Conversion–time curves cannot always be described with existing models, nor can the effects of water vapor pressure and changing crystal structure

Correspondence to: J.A. Lumpkin, Department of Chemical and Biochemical Engineering, University of Maryland, Baltimore County, Baltimore, MD 21228, USA.

always be predicted. The study of dehydration–rehydration kinetics of fully reversible reactions has gained interest because of potential application in chemical heat pump systems employing intermittent absorption cycles [2,3].

For the hydrates that have been studied extensively [4], the focus has generally been on irreversible dehydration reactions, and the modeling is usually limited to either the kinetic or the diffusion limited regime. More recent investigations have included mathematical models of reversible reactions [5,6] and some have included a diffusional term in the rate of interface movement [6]. Since the reactions of interest are reversible and the practical application involves the use of beds of the compounds, the bulk water vapor pressure and the diffusional behavior of water vapor are expected to be important within an individual particle as well as in the sample bed. In addition, crystallization of the product phase or of intermediate hydrates can be promoted by water vapor [7,8]; thus water vapor can promote or retard the reverse reaction. Possible intermediates include known lower hydrates and/or metastable crystalline or amorphous hydrates of various degrees of hydration [8,9]. This effect becomes even more important in view of possible transient increases in water vapor pressure caused by diffusional limitations in large-sized particles, pellets or sample beds. When lower hydrates exist, reaction has usually been studied under conditions where the steps are believed to be distinct; practical circumstances often produce overlapping reactions.

This research addresses the role of diffusion in the dehydration kinetics of the fully reversible reactions of the barium chloride–water system, a promising candidate for chemical heat pump application [2,10]. Special attention was accorded to structural changes in the solids and to the water vapor environment.

BACKGROUND

The $BaCl_2$–H_2O system is generally understood [11–20] to include dihydrates and mononydrates, and the commonly observed reactions are

$$BaCl_2 \cdot 2H_2O(s) \leftrightarrow BaCl_2 \cdot H_2O(s) + H_2O(g) \quad (1)$$

$$BaCl_2 \cdot H_2O(s) \leftrightarrow BaCl_2(s) + H_2O(g) \quad (2)$$

$$BaCl_2 \cdot 2H_2O(s) \leftrightarrow BaCl_2(s) + 2H_2O(g) \quad (3)$$

It should be noted that a hemihydrate has also been reported [21–23], presumably involving the following reactions:

$$BaCl_2 \cdot 2H_2O(s) \leftrightarrow BaCl_2 \cdot 0.5H_2O(s) + 1.5H_2O(g) \quad (4)$$

$$BaCl_2 \cdot H_2O(s) \leftrightarrow BaCl_2 \cdot 0.5H_2O(s) + 0.5H_2O(g) \quad (5)$$

$$BaCl_2 \cdot 0.5H_2O(s) \leftrightarrow BaCl_2(s) + 0.5H_2O(g) \quad (6)$$

As is common with many hydrate systems, most of the research to date has focused on modeling the temperature dependence and the conversion–time behavior of the dehydration reactions in the kinetic controlled regime [14,17,19,24–26]. Most of the reactions were conducted under a flowing nitrogen atmosphere, or the evolved water vapor pressure was allowed to remain in the reaction vessel. Careful control and measurement of water vapor partial pressure were reported in a few cases [3,10,27]. Data on rehydration rates and the effect of multiple reactions (cycling) on reaction kinetics have also been reported [3]. Research has been done on the crystal structure of $BaCl_2 \cdot H_2O$ during dehydration reactions [25,28]; the effect of temperature variations was reported. The water vapor pressure [23], sample type (powder vs. single crystal) [17,24,25], particle size [12,17,26] and thermal history [17,24], as it relates to the hydrate's parent compound, have also been shown to be important factors.

A common finding is that the dehydration of barium chloride dihydrate proceeds in a stepwise manner (dihydrate to monohydrate to anhydrous salt) under isothermal as well as non-isothermal conditions [16,17,19,24,25]. Furthermore, it has been reported that the first dehydration is complete before the second dehydration begins in the temperature range 40–80°C [29]. Thus the reaction kinetics were reported for either the dihydrate to monohydrate reaction or the monohydrate to anhydrous reaction, but not both. One exception was noted by Ingraham and Rigaud [24], who reported that a lack of match of the exponents in fitted kinetic models was believed to be caused by some overlap of the dehydrations in some non-isothermal reactions.

The most commonly used expressions for isothermal decomposition reactions relate fractional conversion α to time t:

$$f(\alpha) = kt \tag{7}$$

The form of the function $f(\alpha)$ and the associated dehydration rate constant k are determined by the rate-controlling process and geometry assumed in the derivation. Table 1 summarizes the conversion expressions most widely applied to dehydration reactions. The results of several previous investigations of the barium chloride–water system are summarized in Table 2.

Vapor pressure data for the dihydrate–monohydrate and monohydrate–anhydrous systems [11,24,30–33] have been obtained by a variety of techniques. Values ranging between 1600–3600 Pa and 93–1600 Pa, respectively, have been reported or calculated at 317 K. Stanish [33] suggested that the scatter in the equilibrium data was probably attributable to a slow transformation rate of the dihydrate to the monohydrate and that systems which employed dynamic analyses were more prone to error.

EXPERIMENTAL APPARATUS AND PROCEDURES

Materials

Reagent grade crystalline powders of barium chloride dihydrate were used in each analysis. The TGA and optical microscopy studies were conducted with barium chloride (Baker) sieved to standard size fractions ranging from 53 to 710 μm; the calorimetry studies were conducted with barium chloride (EM Science) sieved to standard size fractions ranging from 75 to 150 μm.

Thermogravimetric analysis

The dehydration kinetics were monitored on a Cahn 2000 recording electrobalance thermogravimetric analyzer (TGA). The balance and sample pans were housed in a glass assembly within which the gaseous atmosphere

TABLE 1

Conversion expressions for solid state decomposition in the form $f(\alpha) = kt$

Function $f(\alpha)$	Symbol for model	Name of model	Rate-controlling process
Acceleratory conversion – time curve			
$\alpha^{1/n}$	P_n	Power law	Kinetic: n = order
$\ln \alpha$	E_1	Exponential	Kinetic
Sigmoidal conversion – time curve			
$[-\ln(1-\alpha)]^{1/m}$	A_m	Avrami–Erofe'ev	Kinetic: random nucleation $m = 1$ Random nucleation and subsequent growth: $m = 2, 3, 4$ Diffusion: $m = 0.5, 1, 1.5, 2.5$
$\ln[\alpha(1-\alpha)]$	B_1	Prout–Tompkins	Kinetic: autocatalytic
Deceleratory, conversion – time curve			
$1-(1-\alpha)^{1/n}$	R_n	Phase boundary or shrinking core	Kinetic: rate of interface movement n = order
α	D_1	Diffusion-limited shrinking core	1-D diffusion
$(1-\alpha)\ln(1-\alpha)+\alpha$	D_2		2-D diffusion
$[1-(1-\alpha)^{1/3}]^2$	D_3		3-D diffusion
$[1-2/3\alpha-(1-\alpha)]^{2/3}$	D_4	Ginstling–Brounshtein	Diffusion

TABLE 2

Conversion expressions for isothermal dehydration of hydrated barium chloride

Model	Range of validity	Reaction stage
From ref. 17 for powder samples		
P_2	$0 < \alpha < 0.1–0.15$	Dihydrate to monohydrate Monohydrate to anhydrous
A_2	$0.15 < \alpha < 1$	Dihydrate to monohydrate Monohydrate to anhydrous [a]
A_2	$0 < \alpha < 1$	Monohydrate to anhydrous [b]
From ref. 17 for single crystals		
P_2	$0 < \alpha < 0.15$	Dihydrate to monohydrate
R_2	$0.15 < \alpha < 1$	Dihydrate to monohydrate
From ref. 19 for powder samples		
$A_{2.08}$	$0 < \alpha < 1$	Dihydrate to monohydrate
$R_{1.54}$	$0 < \alpha < 1$	Dihydrate to monohydrate
$A_{2.92}$	$0 < \alpha < 1$	Monohydrate to anhydrous
$R_{1.50}$	$0 < \alpha < 1$	Monohydrate to anhydrous

[a] Monohydrate from dehydrated dihydrate.
[b] Fresh monohydrate.

was controlled. A Welch Duo-Seal vacuum pump and a water vapor delivery system were added to the TGA. The vacuum pump was capable of maintaining a vacuum of about 10 Pa. The pressure was monitored with a Serta electronic manometer.

The water vapor pressure was controlled by connecting the TGA assembly to a flask containing distilled water. The assembly was evacuated and purged five times with pure water vapor at (1.6×10^3)–(2.0×10^3)Pa prior to each run. The sample was then heated slowly and allowed to come to thermal equilibrium (about 1 h) under the pure water vapor atmosphere. The dihydrate was stable at this pressure for the temperature range of interest. Dehydration was initiated by closing off the water vapor source and applying a vacuum.

Calorimetry

Dehydration experiments were performed in a Setaram C-80 twin-cell heat-flux calorimeter from which simultaneous kinetic and heat of reaction data were collected. All experiments in this study were conducted under isothermal conditions. Both sample and reference cells were connected to a Hause–Leobold vacuum pump via flexible metal hosing. A Sargent–Welch model 1516 electronic thermocouple vacuum gauge that measures pressures up to 6.67×10^2 Pa was mounted between the cells. The minimum pressure obtained experimentally was 17.3 Pa. The heat of reaction is an

integral quantity that is calculated from the power–time data recorded for the calorimeter.

Kinetic data were determined by dividing the energy exchanged up to a given time by the total heat of reaction. Since the reaction time was in many instances comparable with the instrument's heat transfer time constant of 250 s, the raw data had to be corrected to account for heat transfer limitations [34]. The temperature of the sample vessel's outer wall was continuously recorded in every run to provide a measure of the deviation of the sample temperature from the control temperature. The maximum discrepancy was 0.30 K; typical differences were less than half of this value.

X-ray diffraction

X-ray analyses were performed on a Rigaku Rotaflex diffractometer, using Cu Kα radiation. A thin layer of sample powder was mounted on a glass microscope slide. The X-ray source was a 12 kW rotating anode. The approximate percentage of each material was determined from averaged peak intensities [34].

Optical microscopy

A polarizing microscope equipped with a Mettler FP5/FP52 hotstage and a 35 mm single-lens reflex camera was used to observe and obtain photographs of the reaction interface. The microscope was operated with the polarizers crossed. In this mode of operation an anisotropic (birefringent) material can be positioned in the light beam so that a bright white or colored image appears [35]; however, an isotropic material is dark in all positions. Since barium chloride dihydrate, monohydrate and anhydrous salt have monoclinic, orthorhombic and cubic symmetries, respectively, the progress of the reaction interface can be followed by monitoring the transition from a white or colored to a blackened particle.

The heated stage was operated in the isothermal mode; temperature could be controlled to ± 0.5 K. The stage was sealed and contained gas ports so that a constant nitrogen flow could be maintained throughout the analysis.

MODELING CONVERSION

A kinetic expression was developed which includes diffusion by focusing on the water vapor concentration profile in the sample bed. The one-dimensional unsteady-state Fickian diffusion equation with a time-dependent chemical reaction term may be written as

$$\partial c/\partial t = D\ \partial^2 c/\partial z^2 + \rho(t) \tag{8}$$

where c is the concentration, t the time, D the diffusion coefficient of water in the bed, and $\rho(t)$ the time-dependent reaction rate. The boundary and initial conditions are (1) $c = 0$ at $z = h$ (top of sample bed); (2) $dc/dz = 0$ at $z = 0$ (bottom of sample bed); (3) $c = 0$ at $t = 0$.

Assuming that the reaction rate term is of the form

$$\rho(t) = c_{max} k \, e^{-kt} \tag{9}$$

where c_{max} is the maximum concentration of water vapor available for reaction, the concentration profile is

$$c(z, t) = c_{max} \frac{4k}{\pi} \sum_{n=0}^{\infty} \frac{(-1)^n}{(2n+1)} \cos \frac{(2n+1)\pi z}{2h} \frac{1}{(\kappa - k)} (e^{-kt} - e^{-\kappa t}) \tag{10}$$

where $\kappa = D(2n+1)^2\pi^2/4h^2$.

The position- and time-dependent concentration profile can be used to calculate the water vapor flux as a function of time, and rewritten in terms of the fraction of water that has escaped from the bed [34]. The conversion–time expression is

$$\alpha(t) = \frac{2D}{kh^2} \sum_{n=0}^{\infty} \frac{1}{\left(\frac{\kappa}{k} - 1\right)} \left\{ 1 - \frac{k}{\kappa} - e^{-kt} \left[1 - \frac{k}{\kappa} (e^{-kt})^{\left(\frac{\kappa}{k} - 1\right)} \right] \right\} \tag{11}$$

RESULTS AND DISCUSSION

Diffusional effects

A series of runs with different sample sizes showed the conversion rate to be very dependent on this variable. In both the calorimeter and the TGA, increased sample sizes correspond to deeper sample beds. Figures 1 and 2 compare the conversion results for sample sizes ranging from 10.0 to 48.3 mg (110 to 540 μm bed depth) and from 9.9 to 1609.8 mg (75 to 5×10^4 μm bed depth) in the TGA and the calorimeter respectively. Figure 3 extends the time scale for the slowest reacting sample. In all cases the reaction rate decreases and the shape of the conversion–time curve changes as the sample size increases. For larger sample sizes, a more pronounced inflection point occurs at lower conversion and the rate curves have two distinct regions. Similar results have been observed at 326 and 333 K [34]; however, the sample size at which the shape changes occur decreases as the temperature increases.

Particle size studies (Fig. 4) show that internal diffusional resistance is not significant under moderate vacuum conditions until the particle size exceeds approximately 250 μm. All the sample size studies were conducted with particle sizes ranging from 75 to 150 μm. The relatively simpler

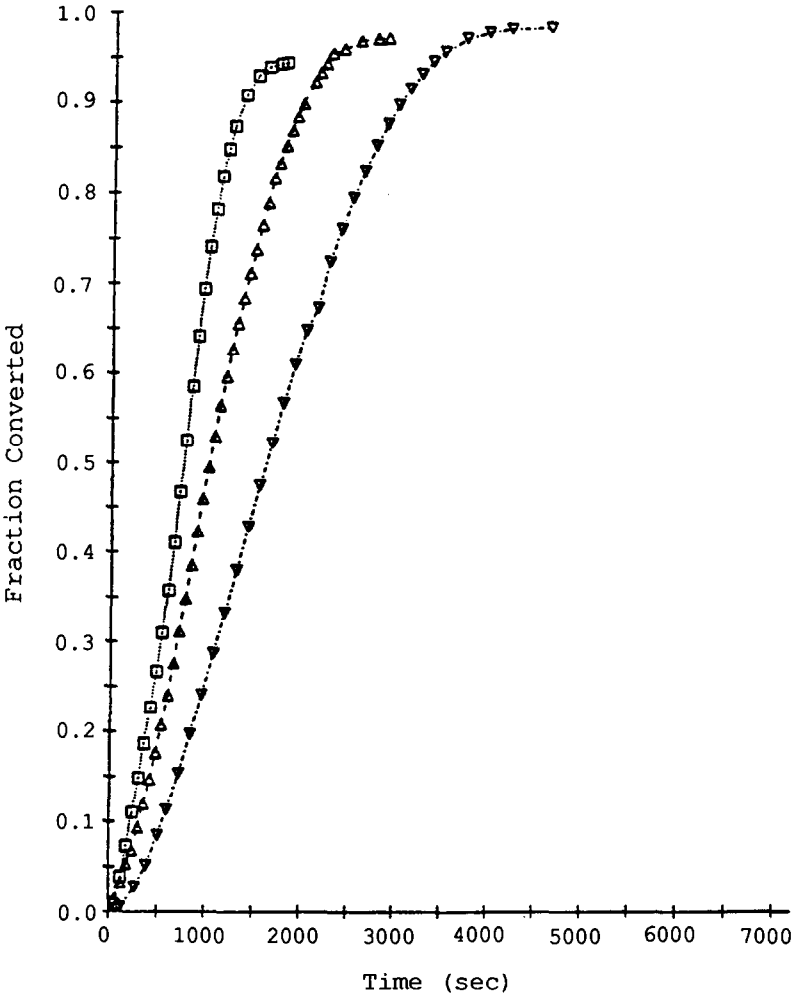

Fig. 1. Effect of sample size (bed depth) on TGA dehydration kinetics at 44°C: □ 10.026 mg; △ 25.503 mg; ▽ 48.345 mg.

development of conversions for the smaller samples may be attributed to the diffusional resistance of the bed of particles to the passage of water vapor. This pattern is to be seen in Figs. 1 and 2 for the shallower beds of approximately 110–600 μm depth. For the 445 mg and larger samples, the water loss proceeded in a stepwise manner rather than by simultaneous loss of the two water molecules of hydration, and produced the sharp "knee" in the curve of conversion with respect to time.

The correlating and predictive powers of the combined kinetic and diffusion model were tested with the TGA data of Fig. 1 for three different bed depths. To carry out such a test it was necessary first to estimate the rate constant k from the data. Assuming that the smallest sample gave a

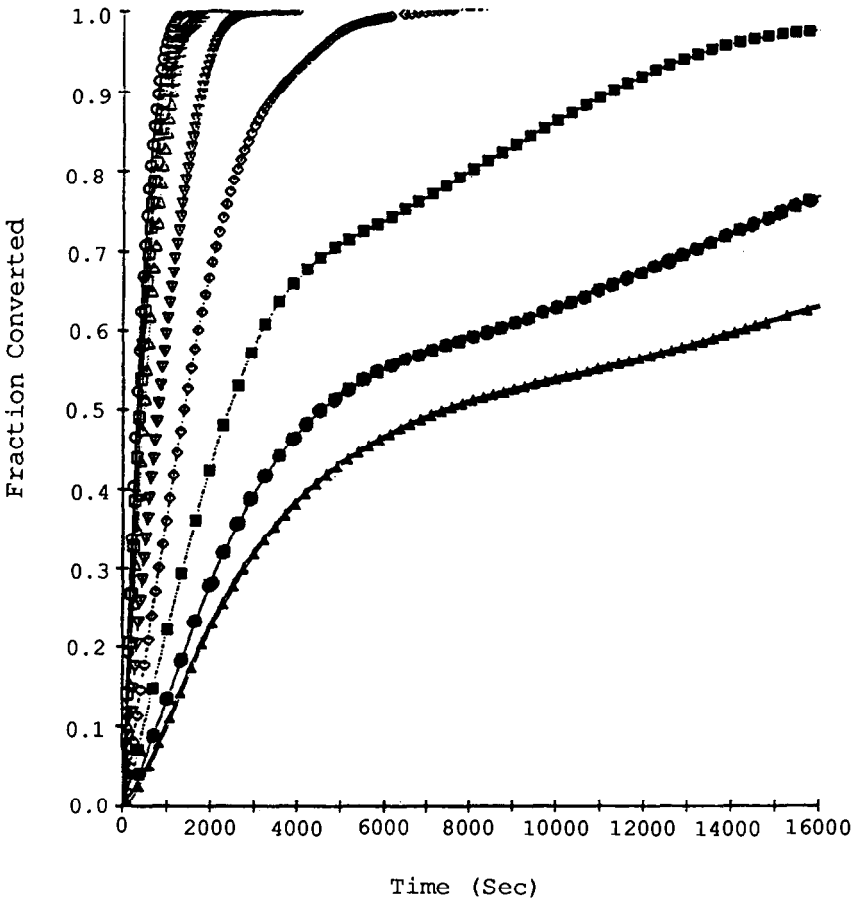

Fig. 2. Effect of sample size (bed depth) on dehydration kinetics in the calorimeter at 45°C: ○, 9.9 mg; □, 19.1 mg; △, 44.6 mg; ▽, 87.4 mg; ◇, 222.5 mg; ■, 446.2 mg; ●, 907.8 mg; ▲, 1609.8 mg.

bed shallow enough to be free of diffusional limitations, the data for the 10 mg sample were fitted to the first-order Avrami–Erofe'ev kinetic expression

$$\alpha(t) = 1 - e^{-kt} \tag{12}$$

The curve fitting was accomplished by a series of iterations by the Marquardt–Levenberg method [36], a combination of the Gauss–Newton procedure and the method of steepest descent, until a least-squares solution was obtained. The fitted curve and the experimental data are shown in Fig. 5 for the rate constant $k = 1.09 \times 10^{-3}$ s^{-1}. Although these data are better fitted by the second-order Avrami–Erofe'ev equation, the simplified model was used to assess the role of diffusion.

The bed diffusion coefficient, $D = 1.0 \times 10^{-6}$ cm^2 s^{-1}, was determined from the 25.5 mg sample in Fig. 1. By using the value for k calculated from

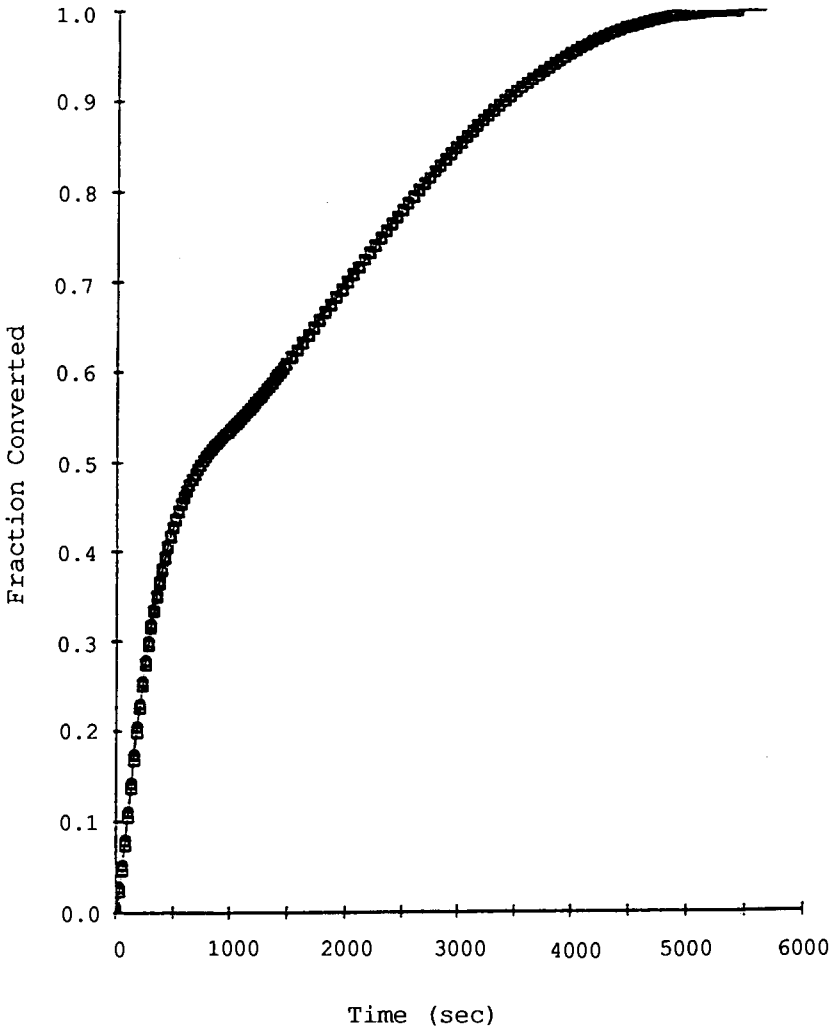

Fig. 3. Extended time scale for dehydration of 1609.8 mg sample in the calorimeter at 45°C.

the smallest sample size (10.0 mg) and the appropriate bed depth ($h = 2.8 \times 10^{-2}$ cm) in eqn. (11), the value of D which gave the best fit to the conversion data in curve 2 was determined. The fitted curve and the experimental points are shown in Fig. 6. Equation (11) was then used successfully to predict the conversion–time curve of the 48.3 mg sample with this diffusion coefficient, the rate constant and the appropriate bed depth, $h = 5.4 \times 10^{-2}$ cm. The experimental data and the theoretical curve are shown in Fig. 7.

The effective diffusivity of 1.0×10^{-6} cm^2 s^{-1} determined from this analysis is comparable with values reported for diffusion through beds of

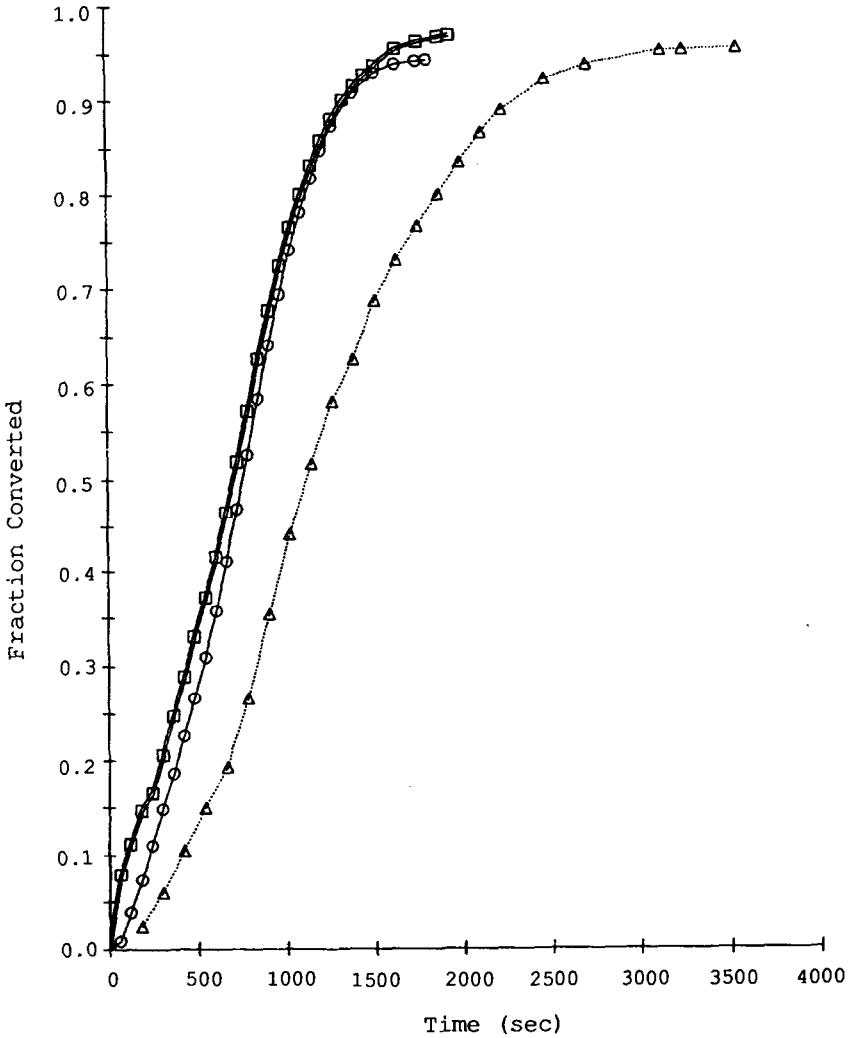

Fig. 4. Effect of particle size on dehydration kinetics at 44°C in vacuum: ○, 53–63 μm; □, 212–250 μm; △, 600–710 μm.

zeolite powders [37]. Since hydrates strongly adsorb water vapor on their surfaces, it is likely that a significant amount of readsorption is occurring as the vapor passes through the sample bed.

The conversion equation (11) is not directly applicable to calorimetric data because the heat and mass transports are not directly coupled, being subject to different boundary conditions. Furthermore, although the diffusion analysis predicts an increase in the transient water vapor pressure with sample bed depth, eqn. (11) cannot predict the stepwise behavior observed in Figs. 2 and 3.

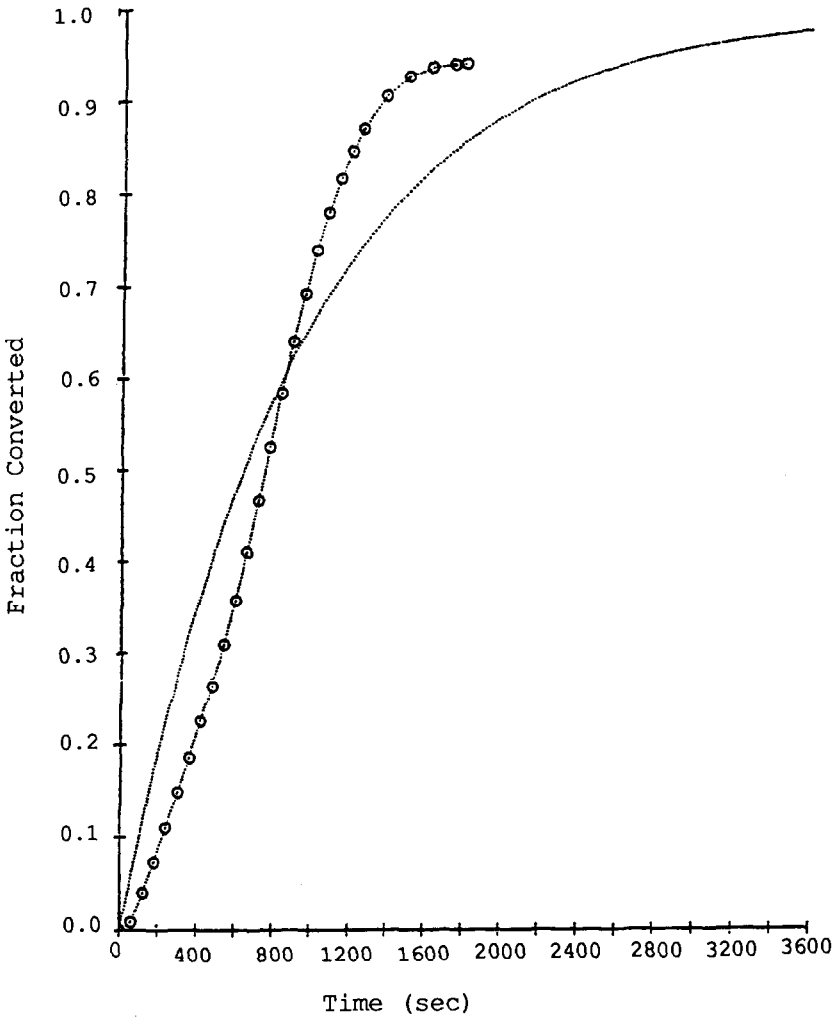

Fig. 5. Fit of first-order Avrami–Erofe'ev model to 10.026 mg sample: o, raw data; ···, $1-\exp(-1.09\times10^{-3}\ t)$.

Effect of transient increases in water vapor pressure

The transition to stepwise dehydration can be understood in part by considering the strong sensitivity of the dehydration rate to water vapor pressure [34]. Although the calorimeter data were collected under a moderate vacuum, the pressure was not constant because of evolving water vapor. The maximum pressure increases for each sample size are listed in Table 3. The maximum pressure increases with temperature at all particle sizes. Over the range of sample sizes analyzed, the maximum pressure increased 2.5-fold and the time required for complete reaction increased by a factor of 32.

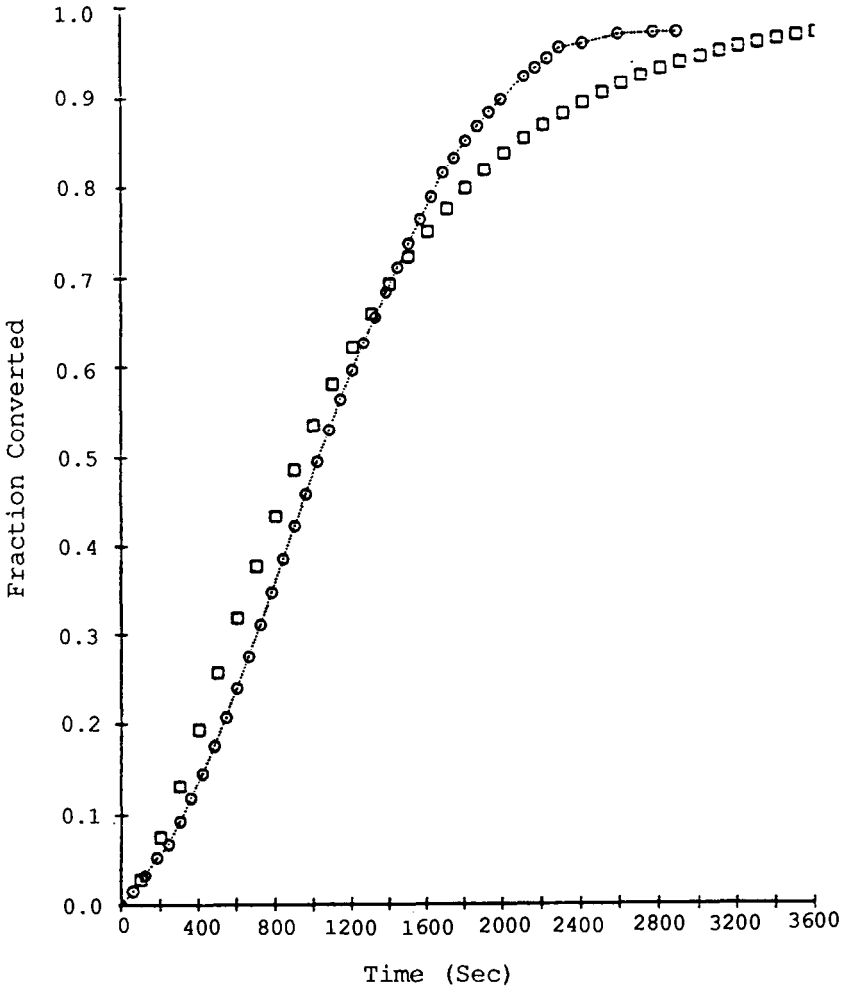

Fig. 6. Best fit of combined diffusion–kinetic control model (eqn. (11)) to 25.5 mg sample: ○, raw data; □ $D = 1.0 \times 10^{-6}$ cm^2 s^{-1}.

An explanation for this phenomenon is that the transient increases in water vapor pressure in the sample bed aided the formation of another hydrate structure which dehydrated at a different rate to the original structure. Since reaction rates fell sharply near 50% conversion, the monohydrate structure may have formed. Strong monohydrate patterns were found in X-ray scans of samples taken from several large sample size (about 1.6 g) runs which slowed and were quenched at conversions near 50%. X-ray scans of samples taken from small samples (about 0.045 g) quenched at 50% and 80% conversion showed mixtures of the dihydrate and anhydrous patterns; the former was approximately 25% dihydrate and 75% anhydrous salt, and the latter was 10% dihydrate and 90% anhydrous.

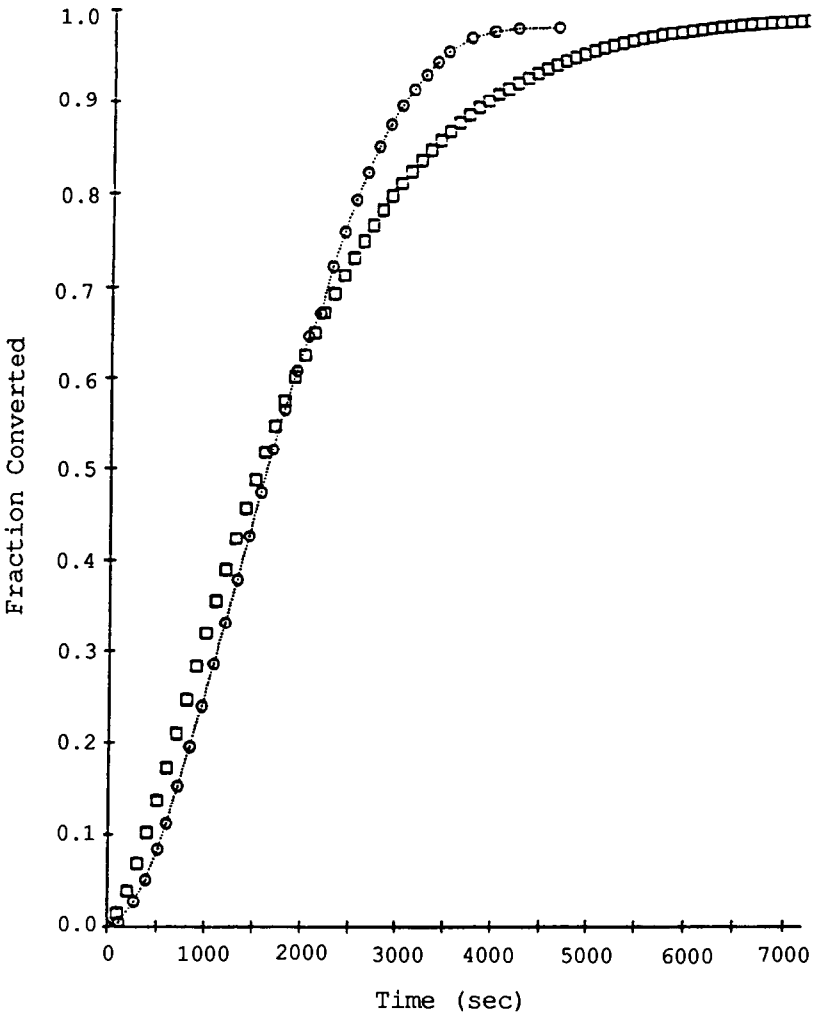

Fig. 7. Fit of combined diffusion–kinetic control model (eqn. (11)) to 48.3 mg sample: ○, raw data; □, eqn. (11).

No evidence of the monohydrate structure was found in these samples. Intermediate-sized samples (about 0.223 g) quenched at 45% and 68% conversion showed mixtures of both hydrates plus the anhydrous salt. The sample quenched at 45% conversion was approximately 34% dihydrate, 39% monohydrate and 27% anhydrous. The sample quenched at 68% conversion was approximately 23% dihydrate, 42% monohydrate and 35% anhydrous.

The changing X-ray scan peaks show that the transient increase in water vapor pressure with sample bed depth resulted in the formation of the monohydrate structure. The lowest reported value for the equilibrium

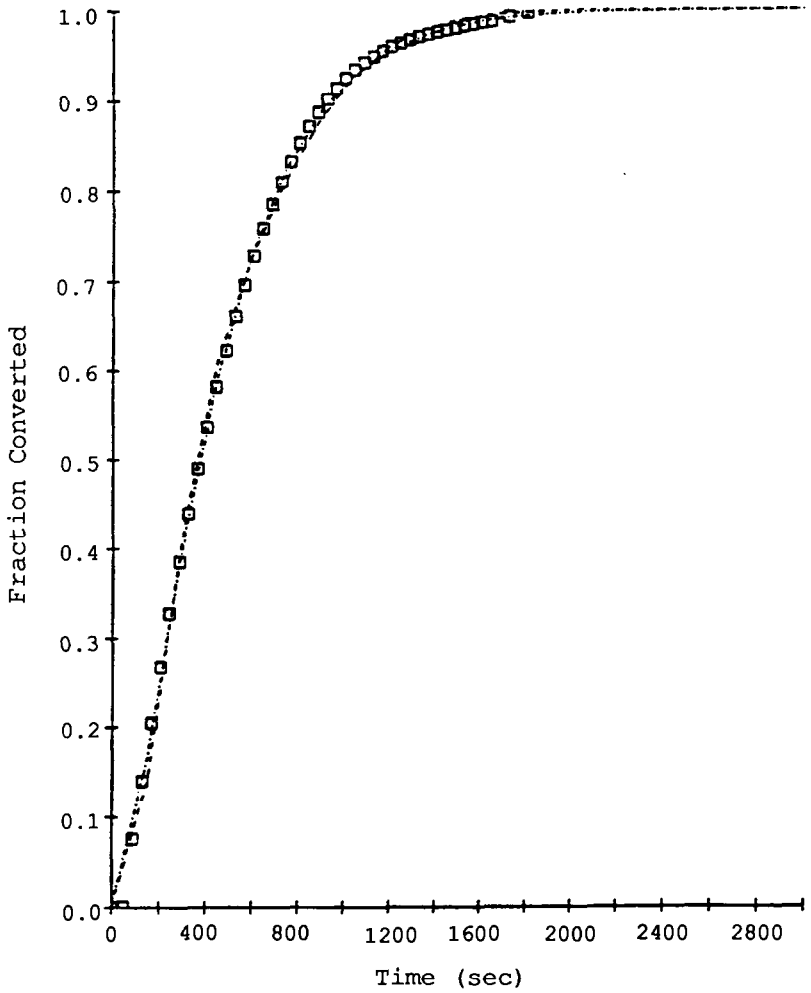

Fig. 8. Fit of overlapping Avrami–Erofe'ev equations of order 1.5 and 2 to conversion–time data of a 19.1 mg sample: □, raw data; - - -, $1-[\exp(-1.25\times10^{-5}t^{2})+\exp(-1.77\times10^{-6}t^{2})]/2$; ·–·–·, $1-[\exp(-1.47\times10^{-4}t^{1.5})+\exp(-5.89\times10^{-5}t^{1.5})]/2$.

vapor pressure of the dihydrate–monohydrate is 93 Pa, comparable with the maximum vapor pressure measured in the larger-sized sample experiments. The production of the monohydrate when large sample sizes are used is consistent with observations to the effect that the dehydration of barium chloride dihydrate proceeds in a stepwise manner via the monohydrate [16,17,19,24,25] and that the first reaction is complete before the second reaction begins in the temperature range 313–353 K [29]. The onset of stepwise behavior at smaller sample sizes for higher temperature dehydrations is consistent with the higher transient water vapor pressures observed (Table 3).

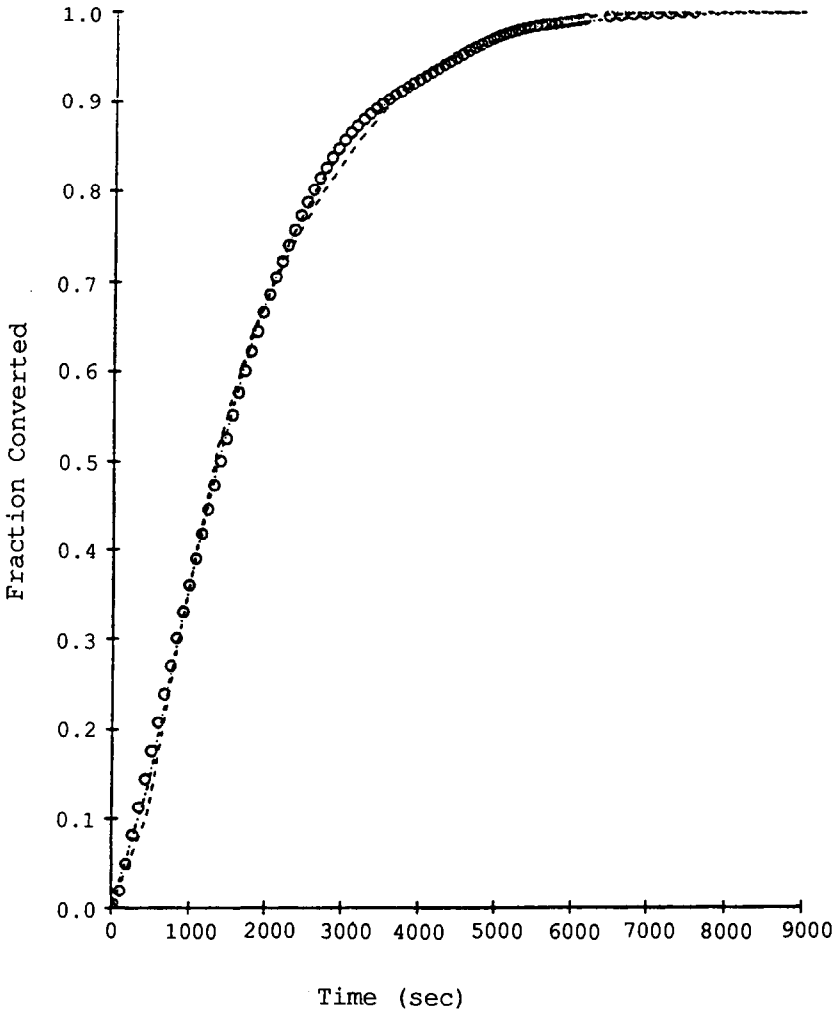

Fig. 9. Fit of overlapping Avrami–Erofe'ev equations of order 1.5 and 2 to conversion–time data of 222.5 mg sample: o, raw data; - - -, $1-[\exp(-9.71\times10^{-7}t^{2})+\exp(-1.24\times10^{-7}t^{2})]/2$; ·-·-·, $1-[\exp(-2.24\times10^{-5}t^{1.5})+\exp(-7.94\times10^{-6}t^{1.5})]/2$.

Kinetic models for overlapping reactions

As noted above, the sample size and particle size studies show that the overall kinetics are in general affected by diffusion. Under the moderate vacuum conditions used in this work the kinetic controlled regime extends to particle sizes of about 250 μm or less (Fig. 4) and bed depths of about 110 μm or less, which correspond to sample sizes of about 10 and 12.5 mg in the TGA and the calorimeter respectively (Figs. 1–3). At higher temperatures and water vapor pressures, the particle size and bed depth must be smaller to remain in the kinetic regime [34].

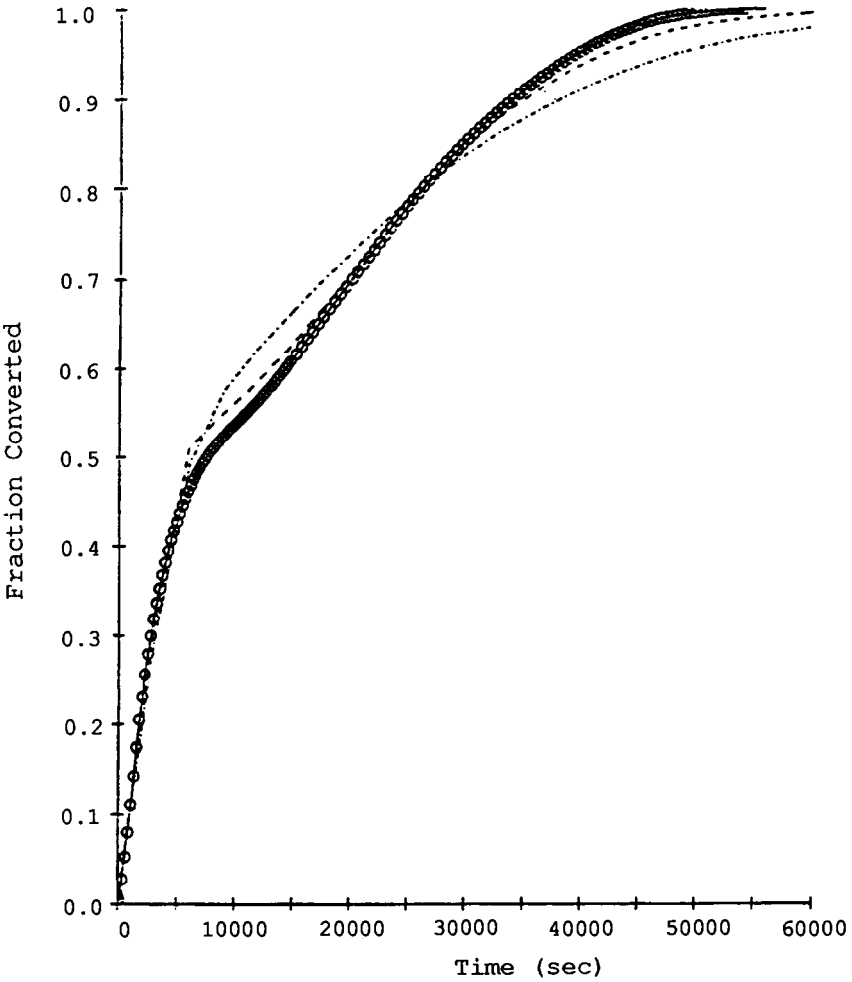

Fig. 10. Fit of overlapping Avrami–Erofe'ev equations of order 1.5 and 2 to conversion–time data of 1609.8 mg sample: o, raw data; - - -, $1-[\exp(-1.02\times10^{-7}t^{2})+\exp(-1.32\times10^{-9}t^{2})]/2$; · – · – ·, $1-[\exp(-4.71\times10^{-6}t^{1.5})+\exp(-2.18\times10^{-7}t^{1.5})]/2$.

The kinetics from 0 to 100% conversion were analyzed in two ways: as a single reaction (simultaneous loss of both water molecules of hydration) and as two overlapping reactions (stepwise loss of both water molecules of hydration). Although the loss of the two water molecules of hydration can occur simultaneously, these water molecules are bound differently [38] and may react at slightly different rates.

The conversion expressions listed in Table 1 apply to single-stage reactions. The expressions for overlapping reactions were derived from a mass balance. Since the two reactions both eliminate one water vapor molecule for each barium chloride hydrate molecule, the water vapor loss is additive,

TABLE 3

Effect of sample size on maximum water vapor pressure observed during reaction

Sample size (mg)	Maximum water vapor pressure (Pa)		
	318 K	326 K	333 K
11.0±1.0	38.7	52.7	67.3
45.0±2.0	42.7	80.0	92.0
88.5±0.7	60.0	81.3	106.7
227.8±5.3	73.3	94.7	121.1
445.0±2.0	80.4	106.7	133.3
908.0±3.0	92.0	118.7	140.0
1607.5±2.5	105.3	125.3	160.0

and the overall conversion α is defined as

$$\alpha = 0.5(\alpha_1 + \alpha_2) \tag{13}$$

where α is the total water lost/maximum water loss possible, α_1 is water lost by the first dehydration/one-half of the maximum water loss possible, and α_2 is water lost by the second dehydration/one-half of the maximum water loss possible.

Thus α, α_1 and α_2 range from 0 to 1. The conversion expression for the Avrami–Erofe'ev equation (eqn. (12)) is

$$\alpha = 1 - [\exp(-k_1 t^m) + \exp(-k_2 t^n)]/2 \tag{14}$$

and the phase boundary equation is

$$\alpha = 1 - \left[(1 - k_1 t)^p + (1 - k_2 t)^q\right]/2 \tag{15}$$

The other conversion expressions are not expressed explicitly in α and have to be determined by iterative techniques.

Tanaka [19] was able to model both reactions by the Avrami–Erofe'ev equation, the first dehydration with $n = 2.08$, the second with $n = 2.92$. The data in this study were analyzed with the single- and two-stage models, seeking the best fits with n and $m = 1$, 1.5, 2 or 3.

The single-stage Avrami–Erofe'ev equation gave relatively high correlation coefficients for the small samples ($n = 1.5$) but was inadequate for the large samples. The two-stage Avrami–Erofe'ev model gave correlation coefficients greater than 0.997 for all the sample sizes with $n = m = 1.5$ and $n = m = 2$. The two forms of the Avrami–Erofe'ev equation were compared with the F test proposed by Green [39] for a significance level of 0.999 [34]. Figures 8–10 show the conversion–time data and the two model curves for three representative samples, 19.1, 222.5 and 1609 mg respectively. The test shows that $n = m = 1.5$ is best for samples of 45 mg and smaller; the remaining samples were best modeled by $n = m = 2$. The rate constants are listed in Table 4.

TABLE 4

Reaction rate constants for overlapping Avrami–Erofe'ev kinetic equations at 45°C

Sample size (mg)	k_1 (s^{-1})	k_2 (s^{-1})
n = m = *1.5*		
9.9	$(1.9 \pm 0.1) \times 10^{-4}$	$(7.8 \pm 0.5) \times 10^{-5}$
19.1	$(1.5 \pm 0.1) \times 10^{-4}$	$(5.9 \pm 0.2) \times 10^{-5}$
44.6	$(8.3 \pm 0.7) \times 10^{-5}$	$(3.4 \pm 0.2) \times 10^{-5}$
87.4	$(3.6 \pm 0.5) \times 10^{-5}$	$(2.6 \pm 0.2) \times 10^{-5}$
222.5	$(2.2 \pm 0.1) \times 10^{-5}$	$(8.0 \pm 0.2) \times 10^{-6}$
446.2	$(1.6 \pm 0.1) \times 10^{-5}$	$(1.4 \pm 0.1) \times 10^{-6}$
907.8 [a]	$(7.6 \pm 0.9) \times 10^{-6}$	$(4.2 \pm 0.2) \times 10^{-7}$
1609.8 [a]	$(4.7 \pm 0.6) \times 10^{-6}$	$(2.2 \pm 0.1) \times 10^{-7}$
n = m = *2*		
907.8	$(1.8 \pm 0.1) \times 10^{-7}$	$(3.1 \pm 0.1) \times 10^{-9}$
1609.8	$(1.0 \pm 0.1) \times 10^{-7}$	$(1.3 \pm 0.1) \times 10^{-9}$

[a] Included to allow for comparison with other samples; second-order model gives better fit.

The differences in reaction order imply that the small- and large-sized sample dehydrations proceed by different mechanisms, in agreement with the X-ray diffraction data. The reaction orders found experimentally are consistent with those of two mechanisms derived for the Avrami–Erofe'ev equations for various nucleation rates and different shapes of nuclei. The reaction orders $n = m = 1.5$ would be expected if a zero-order nucleation rate process occurred for the small-sized samples. The orders $n = m = 2$ are consistent with a decreasing nucleation rate process for the large-sized samples [40]. This would imply that the surface of the dehydrating particles in the small sample runs was covered almost immediately with dehydration nuclei, whereas in larger sample runs most nuclei form early in the dehydration but more form as the reaction progresses. This difference in nucleation rates may occur in the large-sized samples, since they dehydrate under higher water vapor pressures. The additional water vapor would retard the formation of the product phase since the reaction is reversible.

Alternatively, the difference in the time exponent could reflect the difference in the shape of the intermediate transformation products. Zagary et al. [41] have shown, for example, that the water vapor pressure affects the shape of the dehydration nuclei of $CuSO_4 \cdot 5H_2O$. If the nucleation rate is constant, the 1.5 exponent corresponds to thickening plates and an exponent of 2 corresponds to thickening of lengthening rods [42].

Optical microscopy observations of several dehydrating particles showed that nucleation occurred during approximately the first half of the reaction. The dehydrations were not conducted under vacuum but rather under a stream of nitrogen. Under these conditions the dehydration would be

expected to proceed in a stepwise manner, so that the result would be applicable to the larger sample size runs. The results are consistent with the first mechanism described above; however, the second mechanism cannot be rejected entirely, since the reaction conditions differed from those used in the calorimeter runs.

The main differences between the results reported in Table 2 and those found in this work are in the reaction orders obtained. These differences may be caused by differences in the water vapor environment, by reactive intermediates, or by differences in the crystalline state or structure of the starting materials.

ACKNOWLEDGMENTS

The facilities for the bulk of this work were provided by BP America at the Warrensville Research Center, Warrensville Heights, OH. We are particularly grateful to Dr. Jeanette G. Grasselli, Director of Research Science BP America, and Dr. Alex McMaster, Analytical Business Liaison, for their role in arranging access to the facilities. For technical assistance in X-ray diffraction and thermal analysis, we would like to thank Gregory Alexander, Mark Santana, Ernest Armstrong, Martin Mittleman (project leader), Dr. Sampath Iyengar (project leader) and Dr. Phillip Engler (group leader).

REFERENCES

1 A.K. Galwey, N. Koga and H. Tanaka, J. Chem. Soc., Faraday Trans., 86 (3) (1990) 531.
2 M.A. Stanish and D.D. Perlmutter, Sol. Energy, 26 (1981) 333.
3 J.A. Andersson, M. Azoulay and J. de Pablo, Thermochim. Acta, 70 (1983) 291.
4 M. Brown, D. Dollimore and A.K. Galwey, Comprehensive Chemical Kinetics, Vol. 22, Elsevier, Amsterdam, 1980.
5 M.A. Stanish and D.D. Perlmutter, AIChE J., 30 (1984) 56.
6 V.B. Okhotnikov, S.E. Petrov, B.I. Yakobson and N.Z. Lyakhov, React. Solids, 2 (1987) 359.
7 W.E. Garner, Chemistry of the Solid State, Academic Press, London, 1955.
8 N.Z. Lyakhov and V.V. Boldyrev, Russ. Chem. Rev., (Engl. Transl.), 41 (11) (1972) 919.
9 R.M. Dell and V.J. Wheeler, Reactivity of Solids – 5th Int. Symp., Elsevier, New York, 1965.
10 J.A. Andersson, M. Azoulay and J. de Pablo, Int. J. Energy Res., 12 (1988) 137.
11 E.M. Collins and A.W.C. Menzies, J. Phys. Chem., 40 (1936) 379.
12 E.M. Crowther and J.R.H. Coutts, Proc. R. Soc. London, Ser. A, 106 (1924) 215.
13 H.J. Borchardt and F. Daniels, J. Phys. Chem., 61 (1957) 917.
14 M. Rigaud and T.R. Ingraham, Can. Metall. Q., 4 (4) (1965) 237.
15 F. Paulik, J. Paulik and L. Erdey, Anal. Chim. Acta, 41 (1968) 170.
16 E. Buzagh-Gere, S. Gal and J. Simon, in H.G. Wiedemann (Ed.), Therm. Anal., Proc. 3rd Int. Conf., 1971, Birkhaeuser, Basel, 1972.
17 G.G.T. Guarini and R. Spinicci, J. Therm. Anal., 4 (1972) 435.
18 D.A. Skoog and D.M. West, Fundamentals of Analytical Chemistry, Holt, Rinehart and Winston, New York, 1976.

19 H. Tanaka, Thermochim. Acta, 52 (1982) 1.
20 W.W. Wendlandt and E.L. Simmons, Thermochim. Acta, 3 (1972) 171.
21 J. Kessis, C.R. Hebd. Seances Acad. Sci., Ser. C, 264 (1967) 973.
22 V.G. Assarsson, Z. Anorg. Chem., 244 (1940) 330.
23 JCPDS (Joint Committee on Powder Diffraction Standards) Powder Diffraction Files, 1986.
24 T.R. Ingraham and M. Rigaud, Can. Metall. Q., 4 (4) (1965) 247.
25 R.K. Osterheld and P.R. Bloom, J. Phys. Chem., 82 (14) (1978) 159.
26 H. Tanaka and K. Maeda, Thermochim. Acta, 51 (1981) 97.
27 J. de Pablo Ribas and M. Azoulay, An. Quim., 83 (1) (1987) 23.
28 J.L. McAtee, Clays Clay Miner., 18 (1970) 223.
29 Gmelins Handbuch der Anorganische Chemie, System 30, Suppl. Vol., Verlag Chemie, Weinheim, 1960, p. 335.
30 H.W. Foote and S.R. Scholes, J. Am. Chem. Soc., 33 (1911) 1309.
31 G.P. Baxter and W.C. Cooper, J. Am. Chem. Soc., 46 (1940) 923.
32 J.R. Partington, J. Chem. Soc., 99 (1911) 466.
33 M.A. Stanish, Hydration–dehydration kinetics of inorganic salts with potential heat pump applications, Ph.D. Thesis, University of Pennsylvania, 1982.
34 J.A. Lumpkin, Kinetics of the dehydration reactions of hydrated barium chloride, Ph.D. Thesis, University of Pennsylvania, 1988.
35 W.J. Patzelt, Polarized-light Microscopy – Principles, Instruments, Applications, Ernst Leitz Wetzlar, Wetzlar, 1974.
36 Bolt, Berank and Newman, 36 RS/1 User's Guide, Book 2: Graphics and Statistics, BBN Research Systems, Cambridge, MA, 1983.
37 C.N. Satterfield, Heterogeneous Catalysis in Practice, McGraw-Hill, New York, 1980.
38 D.M. Adams, Inorganic Solids – An Introduction to Concepts in Solid-State Structural Chemistry, Wiley, New York, 1974.
39 J.R. Green, Trans. Faraday Soc., 65 (1969) 3288.
40 J.W. Christian, The Theory of Transformations in Metals and Alloys – Part I. Equilibrium and General Kinetic Theory, Pergamon, New York, 1975.
41 A.I. Zagary, V.V. Zyryanov, N.Z. Lyakhov, A.P. Chupakin and V.V. Boldyrev, Thermochim. Acta, 29 (1979) 115.
42 V. Raghaven and M. Cohen, Treatise on Solid State Chemistry – Vol. 5. Changes of State, Plenum, New York, 1975.